Hornblende Gabbro Block in Serpentinite Mélange, Peel-Manning Fault System, New South Wales, Australia: Lu-Hf and U-Pb Isotopic Evidence for Mantle-Derived, Late Ordovician Igneous Activity

R. Offler and S. Shaw[1]

Discipline of Earth Sciences, School of Environmental and Life Sciences, University of Newcastle, Callaghan, New South Wales 2308, Australia
(e-mail: robin.offler@newcastle.edu.au)

ABSTRACT

In the southern New England Fold Belt, the Peel-Manning Fault System (PMFS) is a major structural element characterized by tectonic blocks in a serpentinite mélange. We document a large (>1 km), intensely deformed block of noncumulate and cumulate hornblende gabbro from the PMFS. Cumulate layering is preserved in some outcrops, and relicts of magmatic plagioclase, magnesio-hornblende, and minor clinopyroxene are recognizable microscopically despite the gabbro having undergone amphibolite facies and subsequently prehnite-pumpellyite facies metamorphism. The composition of the magmatic clinopyroxenes and amphiboles indicates low-pressure crystallization, suggesting formation in a shallow crustal reservoir. Zr/TiO_2 ratios, chondrite-normalized rare earth elements ($[La/Yb]_N$ = 6.4–2.7), and rock/MORB (mid-ocean ridge basalt) patterns indicate that the gabbros have a calc-alkaline, basaltic magmatic affinity and a composition transitional between oceanic and continental arc rocks. The mafic rocks intermingled with and intruding the gabbro have a calc-alkaline arc to tholeiitic back-arc basin affinity ($[La/Yb]_N$ = 2.8–1.2). Y/15-La/10-Nb/8 plots confirm the arc affinity of these rocks. Peak metamorphic assemblages formed at temperatures of ~590°C and pressures of 550 MPa, suggesting that a geothermal gradient of ~29°C/km operated during deformation. Single-zircon U-Pb analyses from two rock samples by laser ablation quadrupole inductively coupled plasma mass spectrometry (ICPMS) yielded a combined age of 444.7 ± 2.4 Ma (2σ). Further, Lu-Hf T_{DM} model ages obtained from single zircons from the same samples analyzed by laser ablation multicollector ICPMS were calculated as 447 ± 25 Ma (2σ). The similarity of zircon crystallization ages (U-Pb) and T_{DM} model ages (Lu-Hf) suggests little if any crustal residence between the time of partial melting of depleted mantle to produce the gabbro magma and the time of zircon crystallization. This study provides evidence for Late Ordovician arc magmatism and links all the early Paleozoic arc–related events recognized previously.

Online enhancements: appendix tables.

Introduction

Mélanges containing tectonic blocks in a serpentinite or argillite matrix are common in many high-*PT* metamorphic terrains (Cowan 1978; Nozaka 1999). Their close association with ophiolites and accretion complex and volcanic arc sequences suggests that their formation is in some way involved with subduction processes. Geochemical, metamorphic, and structural studies of the blocks within the mélanges have provided insights into the timing of subduction, exhumation, metamorphic conditions prevailing during subduction, and the tectonic setting of the source from which they were derived (Cowan 1978; Maekawa 1989; Maruyama et al. 1996; Nozaka 1999; Tsujimori and Itaya 1999; De Jesus et al. 2000; Spaggiari et al. 2002).

In the southern New England Fold Belt (SNEFB), New South Wales, Australia (fig. 1), tectonic blocks

Manuscript received March 14, 2005; accepted October 11, 2005.

[1] Department of Earth and Planetary Sciences, Australian Research Council National Key Centre for Geochemical Evolution and Metallogeny of Continents, Macquarie University, Sydney, New South Wales 2109, Australia.

[The Journal of Geology, 2006, volume 114, p. 211–230] 0022-1376/2006/11402-0005$15.00

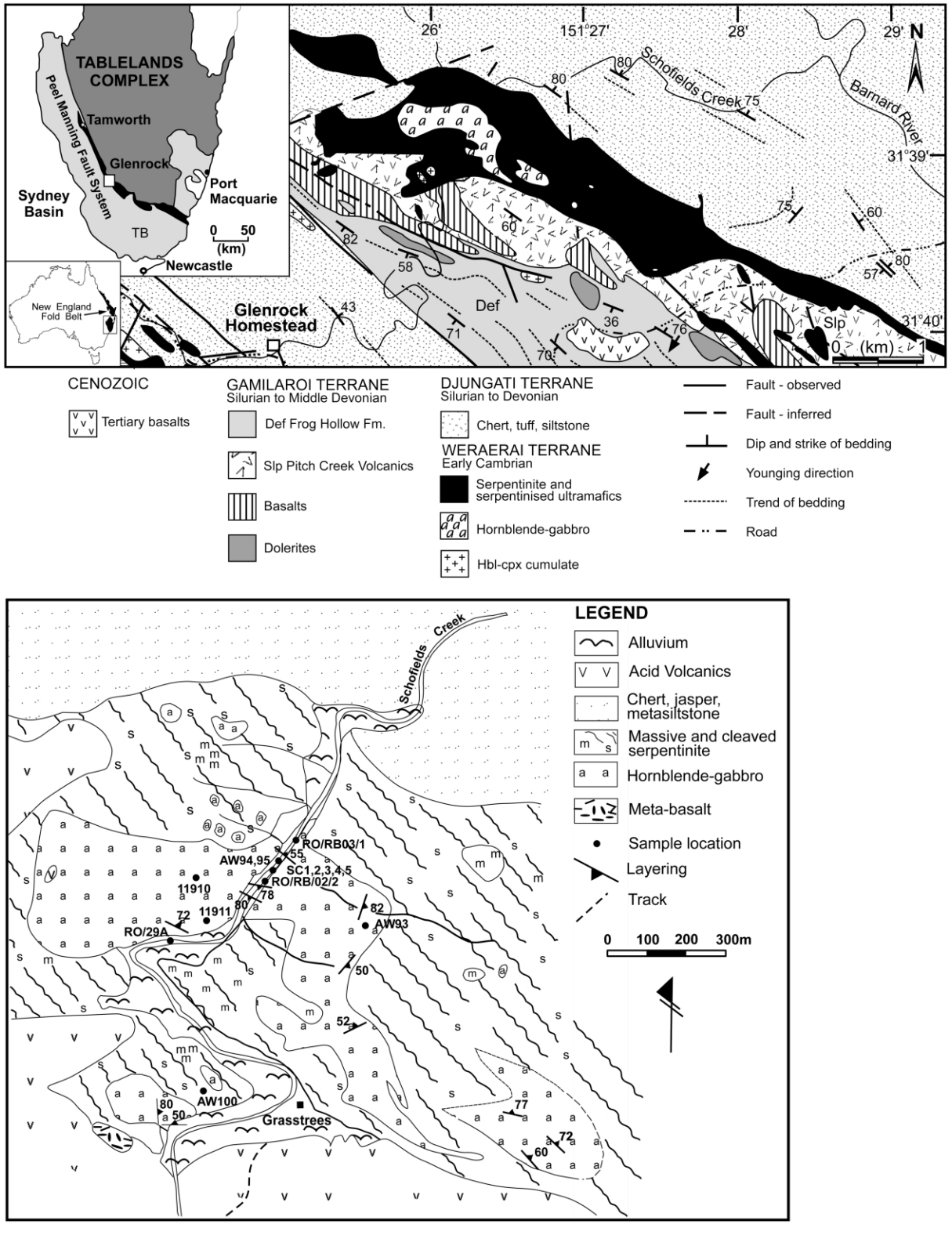

Figure 1. *Top*, geological map showing the location of the hornblende gabbro tectonic block, the serpentinites that enclose it, and the sediments/volcanics of the Gamilaroi and Djungati Terranes (modified from Offler and Gamble 2002). The small inset shows the location of the New England Fold Belt, and the large inset shows the location of the southern New England Fold Belt and study area (Glenrock). *TB* = Tamworth Belt. *Bottom*, geological map of the hornblende gabbro and associated serpentinites, enlarged from top panel.

of varying composition, metamorphic grade, and size occur in a serpentinite mélange. The mélange occurs within the Peel-Manning Fault System (PMFS) or the Great Serpentine Belt of Benson (1913), a major structure that separates the upper Silurian to Carboniferous arc and forearc basin sequences of the Tamworth Belt on the west from the Silurian to lower Carboniferous accretionary-subduction sequences of the Tablelands Complex on the east (fig. 1). It contains fragments of dismembered ophiolite of supra-subduction origin (Aitchison et al. 1994; Yang and Seccombe 1997), the oldest of which is Cambrian in age (U-Pb zircon, 530 Ma; Aitchison and Ireland 1995). Several studies have been carried out on these blocks, particularly the blueschists (Offler 1982, 1999; Cross 1983; Fukui et al. 1995), eclogites (Shaw and Flood 1974; Watanabe and Iwasaki 1988; Allen and Leitch 1992; Watanabe et al. 1998), and amphibolites (Offler 1982). Earlier studies concentrated on petrography, mineral chemistry, and determination of *PT* conditions, and more recent studies on determining the age of metamorphism using K-Ar and U-Pb radiogenic techniques (Fukui et al. 1995; Watanabe et al. 1998; Fanning et al. 2002). However, in only a few of these investigations have the protoliths been determined using major- and trace-element geochemistry (Cross 1983; Offler 1999). Knowledge of the composition of the protoliths and the setting in which they formed is essential in any reconstruction of the tectonic history of the SNEFB.

This article presents major-, trace-, and rare earth element (REE) analyses of a deformed and partly recrystallized hornblende gabbro tectonic block in a serpentinite mélange, Glenrock Station area (fig. 1), together with U-Pb and Lu-Hf single-grain zircon isotopic studies to determine the age, tectonic setting, and source-rock components of this rock. Estimates of the *P-T* conditions prevailing during deformation are also given.

Geology

The hornblende gabbro occurs approximately 3 km northwest of the Glenrock Station homestead, SNEFB (fig. 1), within an Early Cambrian mélange of disrupted, partly or completely serpentinized, supra-subduction zone rocks and tectonic blocks (the Weraerai Terrane; Aitchison et al. 1992, 1994; Aitchison and Ireland 1995; fig. 1) that crop out along the PMFS. Tectonic blocks include blueschists, greenschists, metabasalts, metagabbros, amphibolites, hornblende cumulate rocks, plagiogranite, and locally derived rocks (Offler 1982; Cross 1983; Aitchison and Ireland 1995; Sano et al. 2004). Fault bounded against the serpentinite mélange are Late Silurian to Devonian intraoceanic arc volcanics and volcanogenic sediments (Gamilaroi terrane; Aitchison et al. 1992; Offler and Gamble 2002; fig. 1) and Silurian to Devonian red ribbon-bedded cherts, minor basalts, and volcanogenic sediments (Djungati terrane; Aitchison et al. 1997; Stratford and Aitchison 1997).

Features of the Hornblende Gabbro

The hornblende gabbro consists of a series of irregularly shaped bodies surrounded by schistose and massive serpentinite, the largest >1 km in length. Outcrops are poorly to moderately exposed, with most occurring as well-defined pavements in Schofields Creek (fig. 1). The gabbro is generally highly deformed, with porphyroclasts of igneous plagioclase recognizable in many outcrops associated with an amphibole-rich layering (S_1). Poorly developed asymmetric tails adjacent to some porphyroclasts, typical of mylonites, are observed in some outcrops. Previous descriptions have referred to this body as diorite-amphibolite (Offler and Gamble 2002) and metadiorite (Sano et al. 2004). The hornblende gabbro, although strongly deformed, retains evidence of magmatic crystallization, cumulate layering, and magma interaction (fig. 2). Generally, however, deformation has modified most recognizable igneous features through the development of a strong foliation (S_1) defined by irregularly shaped plagioclase feldspar and amphibole-rich layers 1–3 cm thick that are strongly crenulated in some locations. Overall, S_1 trends NNW to NW, dips steeply SW or NE, and is folded about an axis plunging 82° in a direction 91° (fig. 3*a*). In some outcrops, rare enclaves of magmatically layered cumulates are preserved that vary in size from several to tens of centimeters across. Individual blocks consist of plagioclase-rich and amphibole-rich bands 0.2–4 cm wide alternating in a pattern of cyclic layering (fig. 2) reminiscent of the Skaergaard intrusion. Evidence of convective magmatic erosion, caused by newly formed mineral layers across the cumulate surface of the magma chamber, includes truncated layering and flame-type structures (fig. 2). Locally, mushroom-shaped diapirs of felsic units dome into adjacent mineral layers, and contemporaneous faulting with varying degrees of offset between successive layers is present (fig. 2). In what appears to be a more advanced stage of crystallization, cumulate layering in some blocks has been disrupted by mafic- and felsic-rich differentiates to produce lobate intrusions. The well-developed cumulate layering (S_L) is planar or

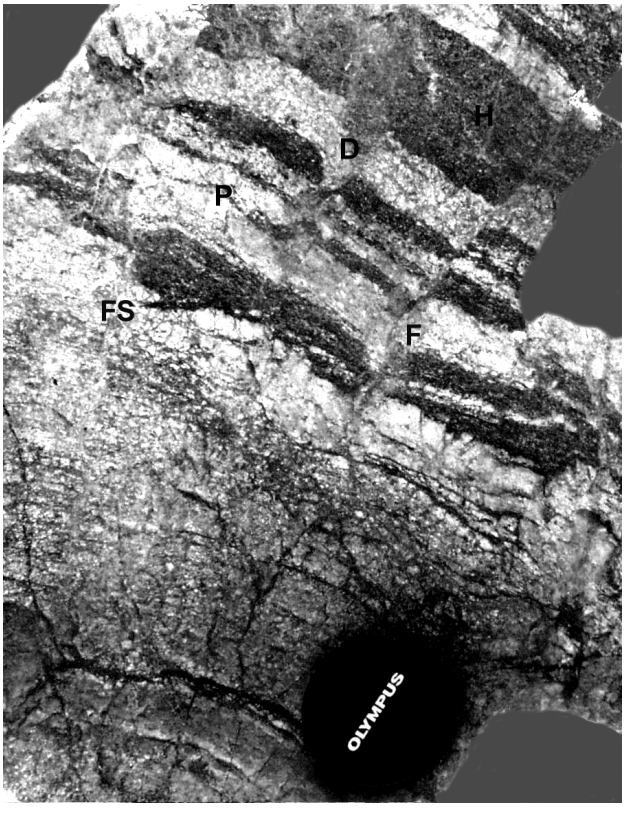

Figure 2. Outcrop photo of cumulate rocks with alternating plagioclase-rich (*P*) and amphibole-rich (*H*) layers. *F* = fault; *FS* = flame structure; *D* = diapir. Younging direction of layers is toward lens cap.

slightly folded and varies in orientation from outcrop to outcrop. In general, S_L is discordant with S_1 and confirms our interpretation that the layered series (S_L) blocks have been tectonically rotated. Intermingled with the layered host are irregular mafic bodies; thin felsic dikes 1.5 cm wide and mafic dikes 1–28 cm wide that trend NW, NNW, and NE also crosscut the host (fig. 3*b*). Contacts between the host and dikes are planar, and those between the host and mafic bodies are cuspate and irregular. In some outcrops, elongate augen-shaped (aspect ratio 4 : 1) and irregular mafic enclaves of variable size occur in the hornblende gabbro, indicating more extensive magma interaction. Close to the northeastern boundary of the outcrop in Schofields Creek, intense epidotization of the gabbro is apparent. The epidote occurs in pods or fractures up to 1 cm thick.

Cutting all outcrops are several generations of shear veins that are intensely developed locally. They commonly exhibit slickenfiber or slickenlines and displace vein arrays, dikes, and crosscut S_1 and S_L, and they rarely develop as conjugate sets. The dominant set strikes NE and dips NW or SE; less common sets trend E–W and N–S (fig. 3*c*). Sinistral strike-slip movement is dominant on the NE-trending veins.

Analytical Methods and Formula Calculations

X-Ray Fluorescence and INAA Analyses. All analyses were done on rock powders produced by grinding rock chips in a Tema tungsten-carbide

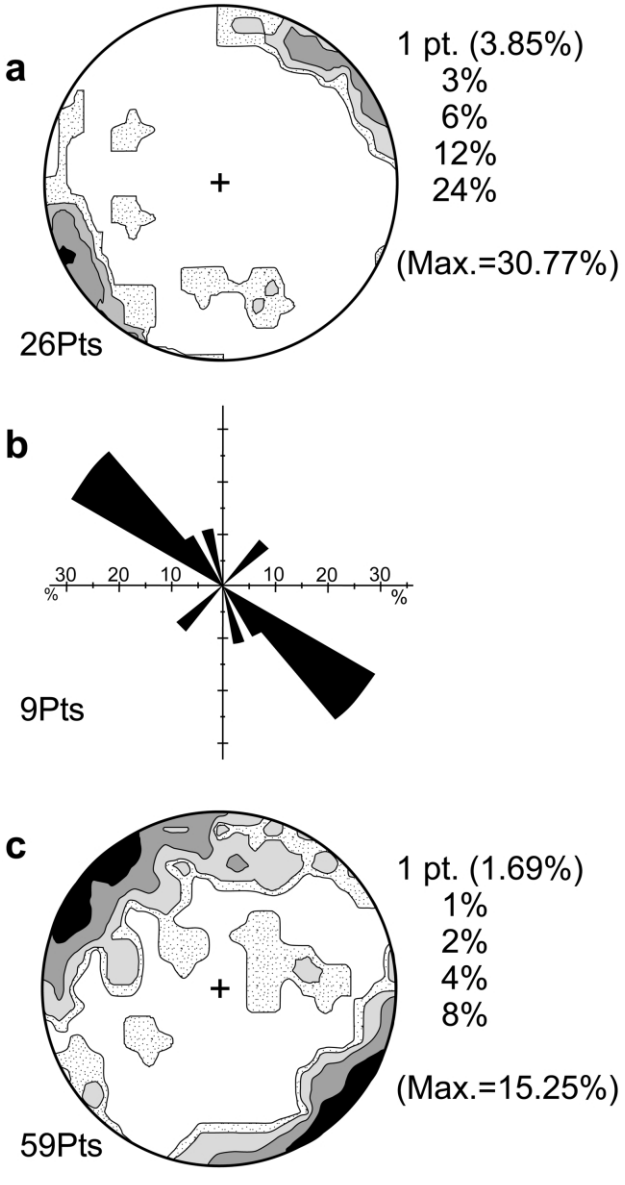

Figure 3. *a*, Layering in hornblende gabbro; *b*, rose diagram showing orientation of dikes; *c*, shear joints in hornblende gabbro.

mill. Ta content was determined from samples ground in a ceramic mortar and pestle. Major and trace elemental analyses were carried out on fused disks (majors) and pressed mounts (traces) at the Victoria University of Wellington, using a Siemens SRS 300 x-ray spectrometer, and at the University of Newcastle, using either a Philips PW 1404 Wavelength Dispersive Sequential XRF or a SPECTRO X-LAB 2000. On some samples, REE, Hf, Ta, and Th content were determined by instrumental neutron activation analysis (INAA) at Becquerel Laboratories, Lucas Heights, and Australian National University, Canberra.

EDS and WDS. The compositions of magmatic and metamorphic minerals were determined using a JEOL JSM-840 SEM (University of Newcastle), attached to which is an Oxford ISIS 200 EDS system, operating at 15 kV and 2.5 mA. Data reduction was carried out on a computer using SEMQUANT. A limited number of analyses to determine the contents of Cl and F in amphiboles were obtained on a Cameca Camebax SX50 at 15 kV, 20 mA (Macquarie University).

Mineral Formula Calculations. Amphibole formulas were calculated on the basis of 23 oxygens and a cation total of 13, excluding (Na+K+Ca). The method of calculating amphibole formulas using a cation total of 15, excluding (Na+K) or K (15-NK), by adjusting Fe^{2+} and Fe^{3+}, was not found to be acceptable for actinolite because Si was overestimated or Ca was allocated to the C site (15-K). All calculations were made using the charge-balance method described by Robinson et al. (1982). Plotting of data was carried out using Minpet, version 2.0, and classification of amphiboles follows Leake et al. (1997).

Zircon Grain Preparation and Analytical Methods. Zircon grains were concentrated from sieved 0.5-mm crushed rock powder of samples SC1 and RO/RB29, using conventional gold-panning dish methods and hand picking with a low-power objective. The selected grains were mounted in an epoxy resin and surface polished. Final identification and selection of zircon was verified by electron microprobe analysis (EMPA). All three analytical procedures (EMPA, U-Pb, and Lu-Hf [$^{176}Hf/^{177}Hf$] isotopic analyses) were conducted on the same epoxy block at the Geochemical Analysis Unit of Macquarie University.

Electron microprobe analyses of Hf, Y, Th, and U, carried out on a Cameca Camebax SX50 at 15 kV and 20 mA, were used to determine compositional variation and the suitability of grains for U-Pb age dating. Table 1 lists the average zircon compositions from samples SC1 and RO/RB29.

Table 1. Average Composition of Zircons

	SC1	RO/RB29A
SiO_2	32.20 ± 1.95	31.93 ± 2.41
HfO_2	1.43 ± .25	1.41 ± .29
ZrO_2	65.51 ± 3.72	65.08 ± 4.51
Y_2O_3	.14 ± .09	.13 ± .10
U_2O_3	.08 ± .05	.06 ± .05
ThO_2	.03 ± .03	.03 ± .03
Total	99.39	98.62

Note. Values are given $\pm 1\sigma$. For SC1, $n = 28$; for RO/RB29A, $n = 49$.

U-Pb age analyses were made by a laser ablation microprobe attached to a quadrupole inductively coupled plasma mass spectrometer (LAM-ICPMS), following the instrumental procedures of Jackson et al. (1996) and using the data reduction program GLITTER (van Achterbergh et al. 2001). Because of the relatively large laser spot size (typically 50 μm), it was impossible to use the same grain for both U-Pb and Lu-Hf isotopic analyses.

Lu-Hf (T_{DM} model age) isotopic analyses were made by LAM-MC-ICPMS, following the method of Griffin et al. (2000) and using in-house data reduction program LAMTRACE. Griffin et al. (2000) developed an elegant correction procedure for $^{176}Hf/^{177}Hf$ in single zircons that allowed an analytical precision of ± 0.00004 (2σ). This corresponds to an ε_{Hf} difference of ~1.5 units, that is, a T_{DM} model age difference of ~50 m.yr.

Structure. Structural data were plotted using the software Georient, designed by R. Holcombe, University of Queensland.

Petrography

Hornblende Gabbro. Samples collected from various outcrops show considerable variation in mineralogy and texture owing to the deformation and associated alteration that have affected the gabbro and the dikes after their emplacement. Magmatic plagioclase is preserved in most samples, but the mafic minerals are commonly replaced by several generations of amphiboles that have different compositions reflecting the varying conditions (upper amphibolite to prehnite-pumpellyite facies) under which they have formed (table 2; fig. 4). Amphiboles of possible magmatic origin show no preferred orientation, replace clinopyroxene (uncommon), and are replaced by metamorphic amphiboles.

In the least deformed samples, euhedral to subrounded magmatic plagioclase occurs that exhibits lobate boundaries (An_{66-71}; sample SC5; table A1, available in the online edition or from the *Journal of Geology* office) and poorly developed zoning. The

Table 2. Mineral Assemblages in Analyzed Samples

	Magmatic					Metamorphic					Veins/alteration products						
Sample	Pl	Amph	Qtz	Ap	Opaque	Pl	Amph	Qtz	Opaque	Ttn	Ep	Prh	Ab	Chl	Cal	Qtz	Opaque
11911	x	x	x	(x)				x		x	x	x	x	x		x	x
AW93[a]	x	x				x	h	x		x	x	x	x	x			x
AW94	x	(x)			x		l			x	x						
AW95	x	x		(x)	(Py)	x	l, h	x	(Ilm)	(x)	x	x	x	x			
SC1	x			x	(x)	x	h			(x)	x	x	x	x	x		
RO/RB02/2	x	x	x	(x)	(x)							x	x				
RO/RB29A	x			(x)		x	l, h			x	x	x	x				x
SC2	x			(x)	(Py)	(x)	h				x	x	x	x			x
RO/RB/02/2D	x		x									x					
RO/RB03/1	x		x									x					
SC3	x	x			(Mt, Py)		l					x	x		x		
11910	x	x				x	l			x	x	x	x	x			x
AW116	x	x				x	l, h			(x)	x	x	x				
AW100							h										
SC4[a]						x	h	x	(Ilm)	x	x	x				x	
SC4 (Leuc)	x		x					x									
SC5[b]	x	x			Py		l		Mt, Ccp	x				x			
99072208B						x	h							x			
99072207	x	x			(Py, Ilm)	x	l		(Mag, Ch)	(x)	x		x	x			

Note. Pl, plagioclase; Amph, amphibole; Qtz, quartz; Ap, apatite; Ttn, titanite; Ep, epidote; Prh, prehnite; Ab, albite; Chl, chlorite; Cal, calcite; Py, pyrite; Ilm, ilmenite; Mt, magnetite; Ccp, chalcopyrite. Minor components are given in parentheses; all others are major components. Leuc = leucosome; l = low grade; h = high grade.

[a] Biotite present.

[b] Clinopyroxene present.

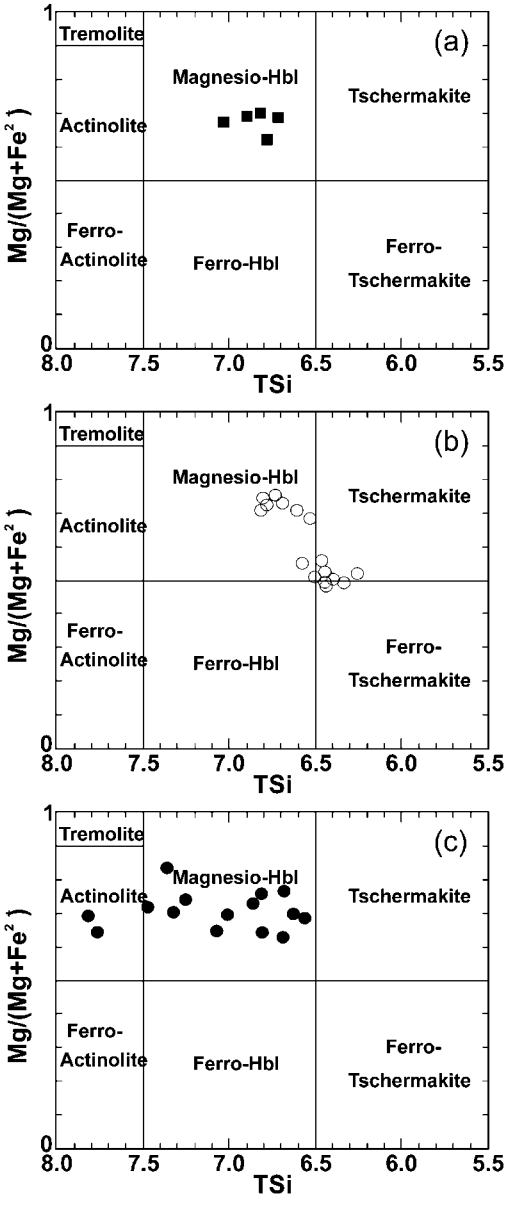

Figure 4. Composition of magmatic amphiboles (*a*), higher-grade metamorphic amphiboles (*b*), and lower-grade metamorphic amphiboles (*c*). Classification after Leake et al. (1997). *Hbl* = hornblende.

subrounded habit of the plagioclase is most apparent in the amphibole-poor and quartz-rich variants. Less commonly preserved are magmatic, Ti-rich, Cl-bearing amphiboles (magnesio-hornblende; table A2, available in the online edition or from the *Journal of Geology* office; fig. 4*a*). The main mafic minerals are metamorphic amphiboles, two or more of which may occur in the same sample (e.g., SC5; 99072208B). Ti-rich, high-grade magnesio-hornblende (Z = green; SC5; table A2; fig. 4*b*) develops earliest and is subsequently replaced by lower-grade, bladed aggregates of less Ti-rich magnesio-hornblende with less intense pleochroism (Z = pale bluish green) and/or actinolite (table A2; fig. 4*c*). The sequential development of these amphiboles suggests that metamorphic conditions changed progressively from upper to lower amphibolite facies and eventually to greenschist or prehnite-pumpellyite facies. In other samples (e.g., 99072208B), tschermakitic hornblende develops. Many grains have zonally arranged magnetite and titanite inclusion trails that are possibly clinopyroxene to amphibole reaction products; others are free of inclusions. Clinopyroxene is rarely preserved and is present in only the least strained rocks as optically continuous patches within magnesio-hornblende (Fs_{15}; SC5; table A1). Quartz is commonly present in magnesio-hornblende as inclusions or as highly strained aggregates in the groundmass. It is a possible by-product of the replacement of clinopyroxene by amphibole. Accessories are apatite, zircon, ilmenite, magnetite, and pyrite; in rare instances, apatite occurs in layers (SC1), suggesting a cumulate origin.

With increasing strain, strongly oriented, finer-grained, Ti-bearing tschermakites (sample AW95; Z = deep green) or magnesio-hornblendes (Z = bluish green; table A2; fig. 4*b*, 4*c*) define S_1 that wraps around magmatic plagioclase. The latter amphibole may also appear in fractures, as idioblastic crystals in plagioclase, and as replacement of the tschermakite and clinopyroxene. Minor dynamic recrystallization of the magmatic plagioclase (An_{43}; AW95) is a feature of some rocks. Magnetite and chalcopyrite are uncommon alteration phases. In rare instances, at very high strains, the gabbro is converted to a strongly foliated amphibolite (SC4) consisting of magnesio-hornblende (Z = slightly bluish deep green), plagioclase ($An_{38.7–41.2}$), and, less commonly, magnetite, titanite, and biotite partly replaced by chlorite. Leucocratic veins discordant with S_1 and containing quartz, euhedral plagioclase ($An_{30.9–31.7}$; table A1), and chloritized biotite are also present. As with most samples in the study area, partial dynamic recrystallization of quartz and, to a lesser degree, plagioclase is manifest in this sample. The presence of igneous textures suggests that the minerals in the veins crystallized from a melt.

Dikes. The mafic dikes show deformation features similar to those of the hornblende gabbros, namely, variable strain, relict igneous textures and minerals, and a variety of metamorphic minerals produced during later deformation events. In the least deformed samples, one or, in some instances, two metamorphic amphiboles (magnesio-

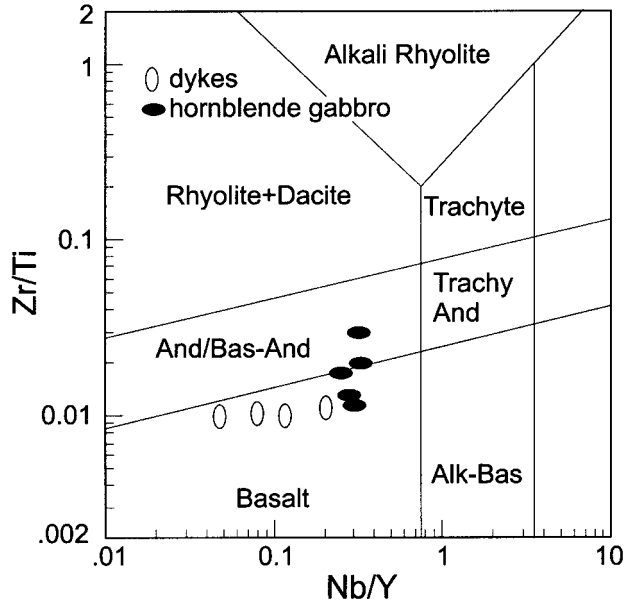

Figure 5. Composition of hornblende gabbro and dikes plotted on the modified Winchester and Floyd (1977) diagram of Pearce (1996). Cumulate rocks are excluded.

hornblende, actinolite) replace what may have been clinopyroxene aggregates or tschermakite, the latter appearing as green cores in metamorphic amphiboles (samples RO/RB29A, SC2). The plagioclase ($An_{58–64}$; table A1) retains a magmatic zoning and occurs as phenocrysts and laths in the groundmass. Secondary pyrite and magnetite are common accessories. With increasing strain, the amphiboles and opaque minerals define a schistosity enclosing plagioclase; zoning is absent. Amygdules, when present, are elongated parallel to the schistosity (RO/RB03/3). By contrast, the felsic dikes retain their igneous texture and mineralogy, namely, quartz and sodic plagioclase, and show minor effects of plastic (undulose extinction, grain boundary suturing, minor dynamic recrystallization) and brittle deformation (vein arrays).

Magmatic Layered Series. Samples of the enclaves (RO/RB/03/5, 9, 10) show alternating amphibole- and feldspar-rich layers; the former are made up of an interlocking aggregate of idioblastic to semi-idioblastic magnesio-hornblende (Z = bluish green) and minor grains of titanite within or at the grain boundaries of the amphiboles. Grain boundaries of the magnesio-hornblende are commonly sutured in highly strained samples, and domainal extinction is well developed. In the feldspar-rich layers, large circular, semicircular, and ellipsoidal subhedral magmatic plagioclase is present. It is partially replaced

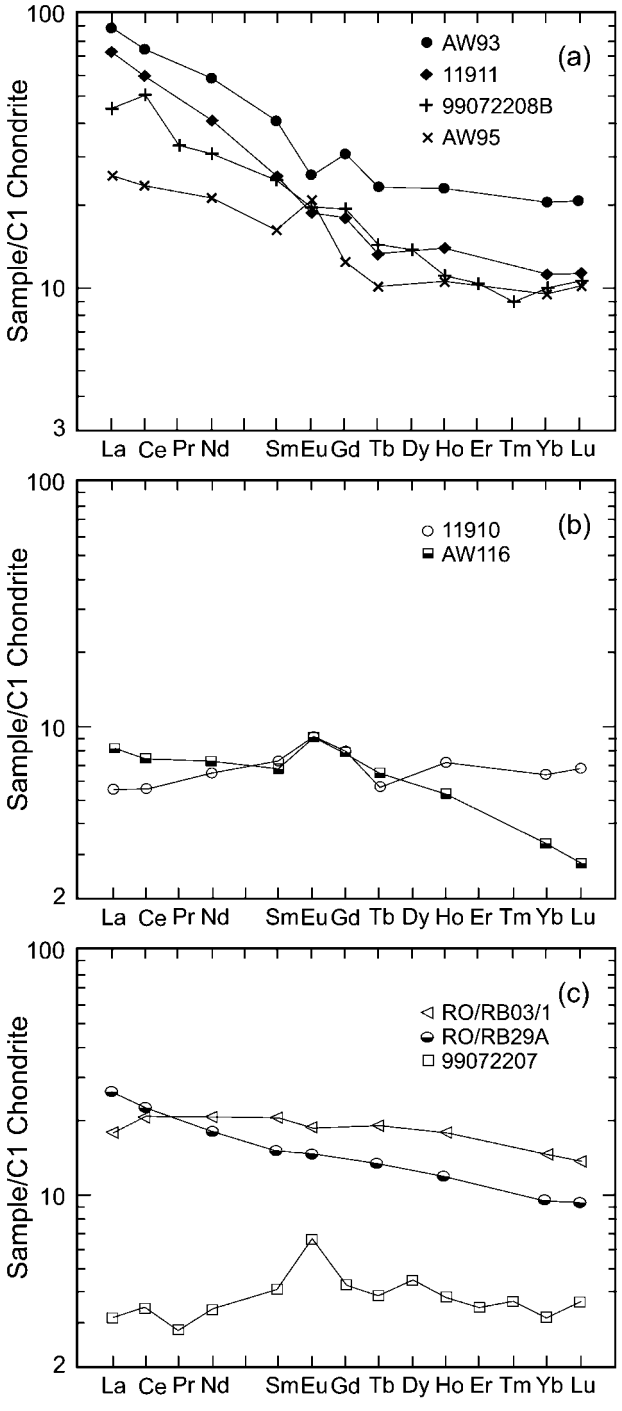

Figure 6. Chondrite-normalized rare earth element patterns. *a*, Hornblende gabbro; *b*, amphibole-rich (AW116) and plagioclase-rich (11910) cumulate rocks; *c*, dikes (RO/RB29A, RO/RB03/1, 99072207). Normalizing values from Sun and McDonough (1989). Data for 99072207 and 9907220/8B are from Sano et al. (2004).

by small dynamically recrystallized plagioclase and surrounded by ribbonlike aggregates of quartz showing subgrain growth and minor recrystallization. Grain boundaries between plagioclase and quartz are typically lobate.

Veins. Overprinting all samples are cataclasite-filled fractures and veins containing one or more of the following in various proportions: epidote, prehnite, chlorite, calcite, albite, and quartz (table 2). Alteration associated with the formation of these veins results in the replacement of magmatic and higher-grade metamorphic mineral phases by actinolite, epidote, prehnite, and chlorite.

Geochemistry: Major Element, Trace Element, and REE. Major-element, trace-element, and REE contents of the gabbros and dikes are presented in table A3, available in the online edition or from the *Journal of Geology* office. The gabbros are dominantly basaltic in composition (fig. 5) and show patterns that are light rare earth element (LREE) enriched (fig. 6*a*; $[La/Yb_N = 6.4–2.7]$). Negative Eu anomalies in some samples (AW93, 11911) and a positive Eu anomaly in AW95 suggest plagioclase fractionation and accumulation, respectively (fig. 6*a*). The mafic dikes are basalts, show higher MgO, Cr, and Ni contents than the gabbros (table A3), and exhibit slightly LREE-enriched ($[La/Yb]_N = 2.8$) or flat chondrite-normalized patterns ($[La/Yb]_N = 0.9$; fig. 6*c*); hornblende-rich cumulate rock (AW116) shows LREE-enriched chondrite-normalized patterns similar to those of the gabbros ($[La/Yb]_N = 2.5$; fig. 6*b*). Plagioclase-rich cumulate rocks, on the other hand, show flat chondrite-normalized patterns ($[La/Yb]_N = 1.0$) and marked positive Eu anomalies, indicating their cumulate origin (11910).

Most rock/MORB (mid-ocean ridge basalt) plots of the gabbro show high field strength element (HFSE) concentrations near that of MORB and enrichment in light lithophile elements (LILEs; fig. 7*a*). The cumulate rocks (AW116; 11910) are depleted in HFSEs relative to MORB, particularly Zr and P, and less enriched in LILE than the gabbros (fig. 7*b*). The strong depletion in Zr and P is a reflection of cumulate formation before zircon and apatite saturation in the melt (Hanchar and Watson 2003). Overall, the dikes exhibit patterns slightly different from the gabbro's in that they are less depleted in HFSE, show less LILE enrichment, and have lower Nb contents (fig. 7*c*). Sample 99072207 is different from other dike samples in that it exhibits a marked positive Eu anomaly and very low REE contents.

Zircon U-Pb and Hf Isotope Data. Typically, zircons vary between 50 and 200 μm in the direction of elongation and, like zircon populations from

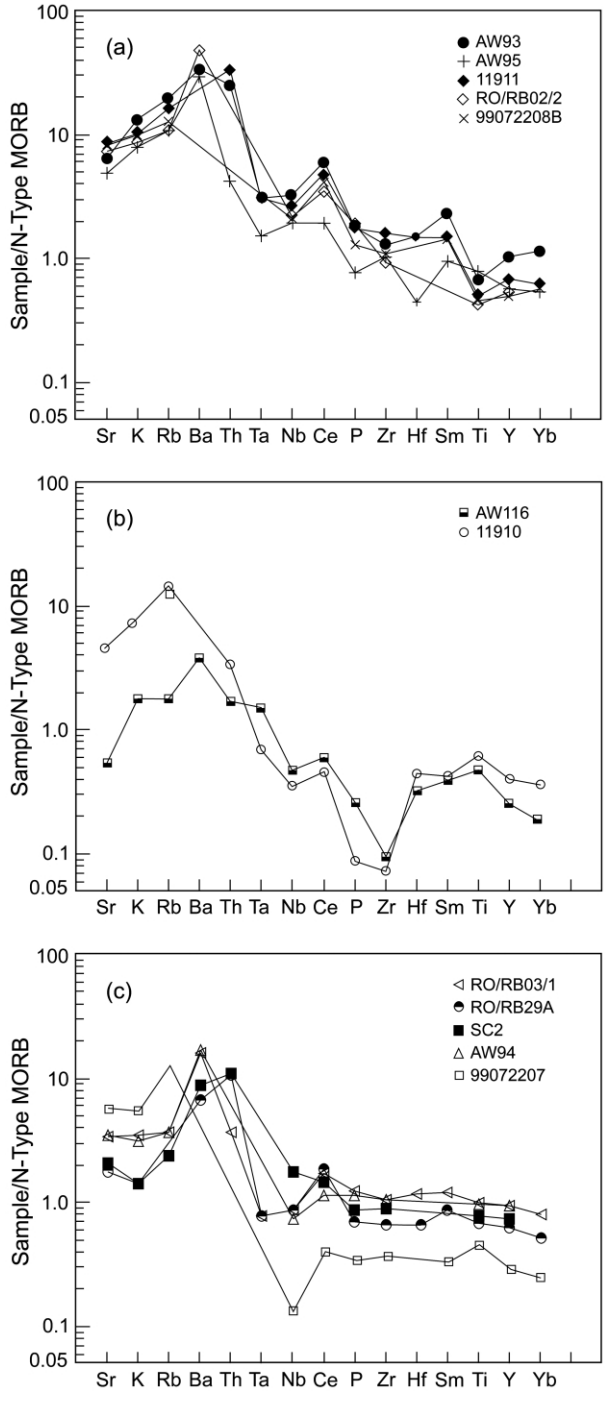

Figure 7. Rock/mid-ocean ridge basalt normalization diagrams. *a*, Hornblende gabbro; *b*, hornblende-rich and plagioclase-rich cumulate rocks; *c*, dikes. Data for samples 99072207 and 9907220/8B are from Sano et al. (2004).

mafic rocks, are anhedral to fragmental (Corfu et al. 2003). Faces of pyramidal form are absent. Backscatter/cathode luminescence electron imaging suggests a complex history that includes fragmentation of once-larger grains and resorption, as indicated by lobate embayments and subsequent regrowth across truncated zoning (fig. 8*A*). Many grains show broad bands of dark and light zoning that traverse the grain (fig. 8*B*). Other fragments lack zoning and appear homogeneous. Grain shape and grain complexity are similar to descriptions, photos, and figures of those found in lower crustal xenoliths, high-grade metamorphic rocks, and kimberlitic rocks (Belousova et al. 1998; Corfu et al. 2003). Compositionally, however, Hf/Y and Y/U abundances are typical of zircons from mafic rocks (e.g., dolerite; figs. 3*a*, 4*a* in Belousova et al. 2002). There is no evidence of metamorphic rimming of any grain, although some boundaries display lobate embayments. This suggests that either the zircon grains are restitic and were entrained in a magma that had not reached zircon saturation temperature (Hanchar and Watson 2003) or changes in T or P_{H_2O} affected the stability field of crystallizing zircon in the melt phase. Influx of a new batch of magma could also be an explanation for these features.

U-Pb age data for SC1 (16 analyses) and RO/RB29 (22 analyses) are presented in table 3 and plotted on a concordia diagram in figure 9. The combined age yields 444.7 ± 2.4 Ma, and the elongation of the error ellipses (fig. 9) indicates Pb contamination that is common but insufficient to displace the majority of points away from concordia.

Table 4 lists the Hf isotopic data from SC1 (10 analyses) and RO/RB29 (9 analyses). The zircon ε_{Hf} values range from +3.47 to +9.90 but group around +5.7. The Lu-Hf model age (T_{DM}) of the combined 19 analyses is 455 ± 28 Ma (2σ), but if analyses (table 4) with a model-age error greater than 44 Ma are excluded, the remaining 12 analyses yield 447 ± 25 Ma (2σ). Because the zircon analyses with larger errors tend to lie at the higher and lower ends of the data range, their exclusion appears justified. Figure 10 is a plot of 12 data points that satisfy the error criteria, the vertical black line of each representing the calculated T_{DM} error.

The U-Pb age of 444.7 ± 2.4 Ma (2σ) is remarkably similar to the Lu-Hf model age (T_{DM}) of 447 ± 25 Ma (2σ), suggesting that magmatic crystallization of zircon closely followed magma generation from depleted mantle. Older T_{DM} ages would imply either greater magma residence time in the crust before crystallization or a source component of older crustal material.

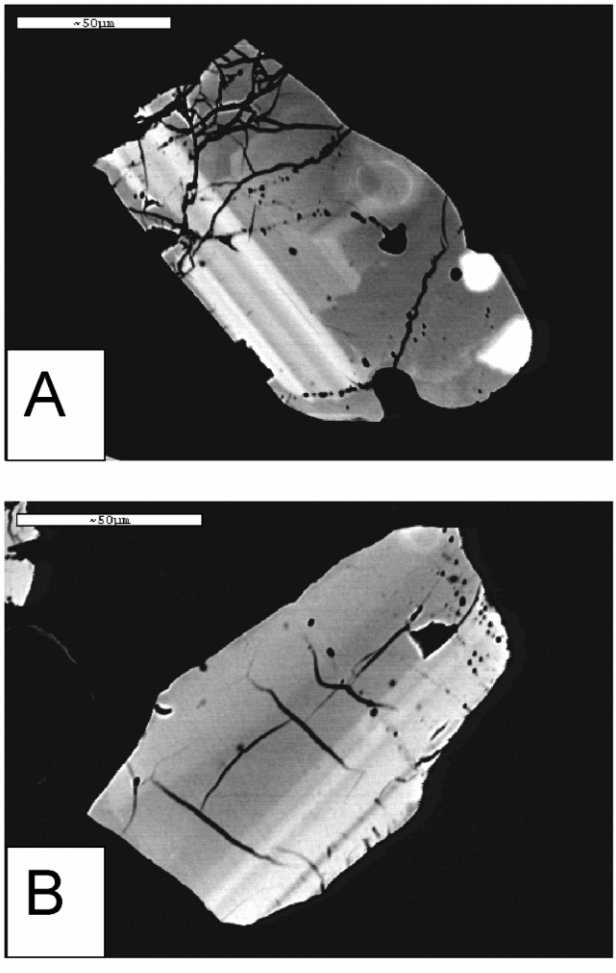

Figure 8. Backscatter/cathode luminescence photographs of zircon grains showing lobate embayments and regrowth across truncated zoning (*A*) and broad bands of light and dark zoning (*B*). Truncated zoning suggests much larger original zircon crystals.

Discussion

Tectonic Setting, Age, and Source. The geochemical data obtained from the gabbro and dikes, in combination with the data collected by Sano et al. (2004), allow constraints to be placed on the tectonic setting in which the gabbro formed. In general, the samples show LREE-enriched chondrite-normalized patterns, high REE contents (fig. 6*a*), and rock/MORB plots characteristic of calc-alkaline arc rocks (fig. 7*a*; Pearce 1983). Further, Y/15-La/10-Nb/8 (Cabanis and Lecolle 1989; fig. 11) and Hf/2-Th-Nb/16 discrimination diagrams confirm the calc-alkaline arc affinity (data not shown; Wood 1980). The slight enrichment in Nb relative to MORB in AW95, the most primitive of the sam-

Table 3. Zircon Pb/U Single-Grain Analyses

	Isotope ratios			Age estimates (Ma)		
	$^{206}Pb/^{238}U$	$^{207}Pb/^{235}U$	$^{207}Pb/^{206}Pb$	$^{206}Pb/^{238}U$	$^{207}Pb/^{235}U$	$^{207}Pb/^{206}Pb$
SC1-2	.06977 ± .00186	.54231 ± .01852	.0563 ± .00176	434.8 ± 11.2	439.9 ± 12.2	463.4 ± 69.2
SC1-3	.07042 ± .00184	.54993 ± .01554	.05654 ± .00136	438.7 ± 11.0	444.9 ± 10.2	472.7 ± 53.0
SC1-4	.06937 ± .00180	.57304 ± .01576	.05976 ± .00138	432.4 ± 10.8	460.0 ± 10.2	594.5 ± 50.3
SC1-7	.07092 ± .00194	.65399 ± .02066	.06672 ± .00184	441.7 ± 11.6	510.9 ± 12.7	829.2 ± 57.3
SC1-8	.07248 ± .00214	.57939 ± .02484	.05789 ± .00234	451.1 ± 12.9	464.1 ± 16.0	525.5 ± 88.1
SC1-9	.07131 ± .00202	.56185 ± .01814	.05705 ± .00156	444.1 ± 12.2	452.7 ± 11.8	493.0 ± 60.6
SC1-11	.07148 ± .00200	.56361 ± .01804	.05712 ± .00158	445.1 ± 12.1	453.9 ± 11.7	495.6 ± 60.6
SC1-12	.07081 ± .00198	.55572 ± .01636	.05688 ± .00136	441.0 ± 11.9	448.7 ± 10.7	486.4 ± 52.8
SC1-13	.07155 ± .00218	.67014 ± .02560	.06793 ± .00232	445.5 ± 13.1	520.8 ± 15.6	866.3 ± 70.3
SC1-14	.07005 ± .00194	.55443 ± .01546	.05735 ± .00126	436.5 ± 11.6	447.9 ± 10.1	504.7 ± 48.0
SC1-15	.07032 ± .00192	.54413 ± .01540	.05608 ± .00128	438.1 ± 11.6	441.1 ± 10.1	455.2 ± 49.6
SC1-16	.06976 ± .00192	.54969 ± .01618	.05709 ± .00140	434.7 ± 11.6	444.8 ± 10.6	494.4 ± 54.0
SC1-17	.07096 ± .00192	.56392 ± .01542	.05758 ± .00126	441.9 ± 11.6	454.1 ± 10.0	513.3 ± 47.0
SC1-18	.07065 ± .00190	.54612 ± .01512	.05601 ± .00124	440.1 ± 11.5	442.4 ± 9.9	452.3 ± 48.3
SC1-20	.07191 ± .00230	.55868 ± .02992	.05636 ± .00296	447.7 ± 13.8	450.7 ± 19.5	465.7 ± 115.6
SC1-21	.07028 ± .00194	.56485 ± .01760	.05823 ± .00154	437.9 ± 11.7	454.7 ± 11.4	537.7 ± 58.8
RO/RB29-1	.07023 ± .00190	.56052 ± .01516	.05786 ± .00122	437.5 ± 11.5	451.9 ± 9.9	524.2 ± 46.3
RO/RB29-2	.07053 ± .00196	.54714 ± .01742	.05624 ± .00154	439.4 ± 11.8	443.1 ± 11.4	461.0 ± 60.1
RO/RB29-3	.07207 ± .00206	.58212 ± .02562	.0585 ± .00250	448.6 ± 12.4	465.8 ± 16.4	548.6 ± 91.6
RO/RB29-5	.07362 ± .00200	.58199 ± .01924	.05731 ± .00170	457.9 ± 12.0	465.7 ± 12.3	502.9 ± 64.3
RO/RB29-6	.07229 ± .00190	.56791 ± .01534	.05694 ± .00126	449.9 ± 11.4	456.7 ± 9.9	488.5 ± 49.0
RO/RB29-7	.07297 ± .00192	.55681 ± .01564	.05531 ± .00130	454.0 ± 11.5	449.4 ± 10.2	424.6 ± 51.7
RO/RB29-8	.07095 ± .00194	.56952 ± .02240	.05811 ± .00220	441.9 ± 11.6	457.7 ± 14.5	533.4 ± 82.7
RO/RB29-9	.07164 ± .00188	.552 ± .01642	.05587 ± .00144	446.0 ± 11.3	446.3 ± 10.7	447.0 ± 56.1
RO/RB29-10	.07253 ± .00190	.58684 ± .01764	.05866 ± .00156	451.4 ± 11.4	468.8 ± 11.3	554.7 ± 57.3
RO/RB29-10A	.0726 ± .00192	.55623 ± .01684	.05557 ± .00148	451.8 ± 11.5	449.1 ± 11.0	434.8 ± 57.8
RO/RB29-10B	.07253 ± .00190	.62485 ± .02024	.0625 ± .00186	451.4 ± 11.5	492.9 ± 12.6	691.2 ± 62.6
RO/RB29-11	.07219 ± .00184	.56074 ± .01490	.05639 ± .00124	449.3 ± 11.1	452.0 ± 9.7	467.0 ± 48.9
RO/RB29-12	.07152 ± .00182	.55976 ± .01460	.05679 ± .00122	445.3 ± 11.0	451.4 ± 9.5	482.8 ± 47.5
RO/RB29-13	.07576 ± .00208	.63226 ± .01910	.06057 ± .00156	470.7 ± 12.4	497.5 ± 11.9	624.0 ± 55.0
RO/RB29-14	.07325 ± .00192	.58282 ± .01790	.05777 ± .00158	455.7 ± 11.5	466.3 ± 11.5	520.9 ± 59.7
RO/RB29-15	.07231 ± .00184	.57827 ± .01530	.05802 ± .00128	450.1 ± 11.1	463.3 ± 9.8	530.0 ± 48.6
RO/RB29-16	.07175 ± .00186	.55861 ± .01730	.05651 ± .00156	446.7 ± 11.2	450.6 ± 11.3	471.7 ± 61.4
RO/RB29-17	.07253 ± .00182	.56061 ± .01440	.05608 ± .00120	451.4 ± 10.9	451.9 ± 9.4	455.3 ± 46.4
RO/RB29-18	.06902 ± .00190	.5265 ± .02090	.05539 ± .00210	430.3 ± 11.5	429.5 ± 13.9	427.7 ± 82.1
RO/RB29-18A	.07186 ± .00182	.56513 ± .01648	.05707 ± .00148	447.4 ± 11.0	454.9 ± 10.7	493.5 ± 57.3
RO/RB29-19	.07137 ± .00178	.55557 ± .01462	.05648 ± .00128	444.4 ± 10.7	448.6 ± 9.5	470.4 ± 50.1
RO/RB29-19A	.07137 ± .00176	.55489 ± .01532	.0564 ± .00140	444.4 ± 10.6	448.2 ± 10.0	467.2 ± 54.6

Note. Values are given $\pm 2\sigma$.

ples (fig. 7*a*; $Zr/TiO_2 \times 0.0001 = 0.008$), and Ta/Yb ratios (0.08–0.21) suggest that these rocks have compositions transitional between oceanic and continental arc basalts (Pearce 1983). The calc-alkaline arc character is also reflected in their V/Ti ratios (fig. 12). Chondrite-normalized REE and rock/MORB patterns and La/10-Y/15-Nb/8 contents (fig. 11) of the mafic dikes confirm the arc setting. However, they show greater variability in composition and magmatic affinity than their hosts (fig. 11). Further, they have lower Nb and LILE contents, and three of the samples (RO/RB03/1, AW94, and RO/RB/29A) have V-Ti/1000 ratios and rock/MORB plots resembling back-arc basin basalts (Gamble et al. 1993). If the chemical signatures of the dikes are a true indication of their tectonic setting, then the dikes must be younger than their host and may reflect the early stages of extension of the arc below which the gabbros formed.

The presence of cumulates as well as clinopyroxenes and amphiboles with compositions reflecting low-pressure crystallization (clinopyroxenes: $Al^{vi} = 0.019–0.029$; table A1; amphiboles: $Al_2O_3 = 7.97–9.04$, $Ti = 0.178–0.248$; table A2; DeBari and Coleman 1989; Ernst and Liu 1998) suggests that crystal growth and settling took place in a magma reservoir at shallow depths beneath the arc. Contact relationships between the gabbro and some of the mafic intrusions show that intermingling took place in the chamber.

The U-Pb data obtained from zircons indicate a Late Ordovician crystallization age for these rocks. Depleted-mantle Lu-Hf model ages (T_{DM}) are similar and confirm that the gabbro was derived

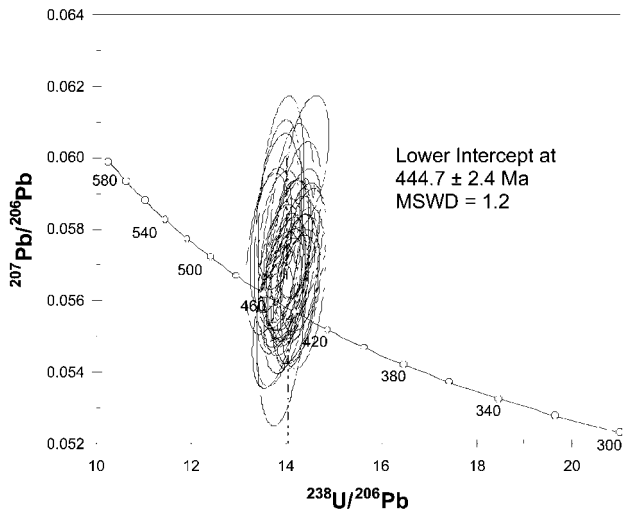

Figure 9. Combined concordia plot of zircon ages from samples SC1 (n = 16) and RO/RB29 (n = 19).

from an isotopically primitive mantle source that, according to Sano et al. (2004), was depleted (Nd_{445} = 0.5). The dominance of amphiboles with minor Cl contents in the gabbro indicates that at the time it crystallized, the magma was extremely hydrous and Cl bearing. Such a magma could have been derived from a mantle wedge contaminated by saline fluids sourced from the slab (Kent et al. 2002). However, further studies are necessary to confirm this.

PT Conditions

Magmatism. The moderately high TiO_2 and low Al_2O_3 contents of the amphiboles (table A2) indicate very low pressure and high temperature of crystallization (P = 100–200 MPa; T = 800°–875°C; Ernst and Liu 1998). The pressure estimates are supported by the Ti-Al^{iv} variation shown in figure 13, which closely corresponds to the variation shown by magmatic amphiboles at pressures between 100 and 300 MPa (Colombi 1989; Zenk and Schulz 2004). However, the temperatures of 800°–875°C suggested by the Al_2O_3, TiO_2, and Ti contents of these amphiboles (Helz 1973; Ernst and Liu 1998) must be regarded as minimum because these contents have replaced clinopyroxene.

Metamorphism. In contrast to the magmatic amphiboles, those developed during the metamorphic events are richer in Al_2O_3 and poorer in TiO_2 (fig. 13), suggesting that pressures increased and temperatures decreased during deformation and alteration of the gabbro and mafic dikes (Ernst and Liu 1998). However, pressures did not increase dramatically;composition plots of Laird and Albee (1981) indicate that all metamorphic amphiboles plot in a zone where medium- (kyanite-sillimanite) and low-pressure (andalusite-sillimanite) facies series overlap (data not shown). This is confirmed by the Si and Al contents of the amphiboles, which suggest that pressures of 550 MPa (range 481–606 MPa; x = 13; σn = 40 MPa) existed during metamorphism, according to the thermobarometer of Gerya et al. (1997).

The temperatures prevailing during metamorphism have varied because amphiboles of different composition formed during different events. The earlier high-grade metamorphism took place at high temperatures, as evidenced by the quartz-plagioclase-biotite–bearing leucosomes present in some rocks (e.g., SC4). To determine temperatures of melting, we used the H_2O-saturated tonalite system of Johannes and Holtz (1996) to allow for the presence of biotite in the leucosomes. Based on the anorthite content of the plagioclase (An_{30}) in the leucosome, and assuming P = 500 MPa and H_2O-saturated conditions, temperatures of ~690°C are indicated. Temperatures of 714°C, determined from coexisting magnesio-hornblende and plagioclase (An_{40}) in the amphibolitic host (Holland and Blundy 1994), are in accord with this estimate. However, these temperatures conflict with those indicated by the thermobarometer of Gerya et al. (1997), namely, 594°C (range 559°–625°C; x = 13; σn = 24°C). We believe that the lower temperature is more realistic because the geothermal gradient of 29°C/km, determined on the assumptions that P = 550 MPa and 100 MPa = 3.7 km, is in accord with the conditions suggested by the compositional plots of Laird and Albee (1981).

Formation in many samples of low-Ti-bearing, bluish-green magnesio-hornblende suggests that temperatures fell after peak metamorphic conditions were attained because Ti contents are controlled by the temperature-dependent substitution $^{[6]}Ti\ ^{[4]}Al_2\ ^{[6]}Mg_{-1}\ ^{[4]}Si_{-2}$ (Ernst and Liu 1998). Estimation of temperatures of formation for these amphiboles is not possible because they show compositional heterogeneity and because plagioclase that formed synchronously with these amphiboles could not be found. The presence of actinolite in most samples and later crosscutting veins with prehnite-pumpellyite facies assemblages suggests that temperatures fell to <350°C, the upper temperature limit for prehnite-epidote-chlorite assemblages (Powell et al. 1995).

The presence of amphiboles formed under lower temperatures and the ubiquitous occurrence of

Table 4. Zircon $^{176}Hf/^{177}Hf$ Single-Grain Analyses

	$^{176}Hf/^{177}Hf$	$^{176}Lu/^{177}Hf$	$^{176}Yb/^{177}Hf$	ε_{Hf} (0)	Crystallization age (Ma)	$^{176}Hf/^{177}Hf$ (initial)	ε_{Hf} (initial)	T_{DM} model age (Ma)
SC1-H1	.282939 ± .000022	.001398 ± .000072	.041432 ± .001800	6.01	439	.282927	15.60	434 ± 33
SC1-H2	.282907 ± .000019	.000897 ± .000220	.029159 ± .007600	4.88	439	.282899	14.62	472 ± 29
SC1-H3	.282933 ± .000026	.001569 ± .000240	.043129 ± .006800	5.80	439	.282920	15.33	444 ± 40
SC1-H4	.282934 ± .000030	.000589 ± .000032	.017136 ± .000960	5.84	439	.282929	15.66	431 ± 43
SC1-H5	.282918 ± .000024	.000933 ± .000078	.025643 ± .001900	5.27	439	.282910	14.99	457 ± 35
SC1-H6	.282885 ± .000030	.000809 ± .000220	.019652 ± .005200	4.10	439	.282878	13.86	501 ± 45
SC1-H7	.282892 ± .000028	.001028 ± .000118	.030174 ± .003800	4.35	439	.282883	14.04	494 ± 41
SC1-H8	.282867 ± .000040	.000926 ± .000220	.022696 ± .006000	3.47	439	.282859	13.19	527 ± 60
SC1-H9	.282881 ± .000030	.000816 ± .000220	.022142 ± .006800	3.96	439	.282874	13.72	506 ± 45
SC1-H10	.282895 ± .000034	.000448 ± .000020	.014869 ± .000700	4.46	439	.282891	14.33	482 ± 48
RO/RB29-H1	.282981 ± .000024	.001379 ± .000050	.057713 ± .002600	7.50	445	.282969	17.22	375 ± 35
RO/RB29-H2	.282890 ± .000022	.000606 ± .000066	.021450 ± .002600	4.28	445	.282885	14.24	491 ± 32
RO/RB29-H3	.282877 ± .000032	.000406 ± .000064	.015989 ± .002600	3.82	445	.282873	13.84	506 ± 46
RO/RB29-H4	.282928 ± .000026	.001200 ± .000040	.045705 ± .001400	5.62	445	.282918	15.40	447 ± 38
RO/RB29-H5	.282981 ± .000024	.001253 ± .000070	.048775 ± .003600	7.50	445	.282970	17.26	374 ± 35
RO/RB29-H6	.282905 ± .000054	.000764 ± .000072	.028888 ± .002200	4.81	445	.282898	14.72	473 ± 77
RO/RB29-H7	.283049 ± .000036	.001616 ± .000220	.057640 ± .008000	9.90	445	.283035	19.56	282 ± 54
RO/RB29-H8	.282918 ± .000026	.000505 ± .000034	.016643 ± .000740	5.27	445	.282914	15.26	452 ± 37
RO/RB29-H9	.282899 ± .000022	.000752 ± .000044	.023763 ± .001100	4.60	445	.282893	14.51	481 ± 32

Note. Values are given $\pm 2\sigma$. Constants used: $^{176}Hf/^{177}Hf$ (DM), 0.28325; $^{176}Lu/^{177}Hf$ (DM), 0.0384; 176Lu decay donstant (yr), $1.93E^{-11}$.

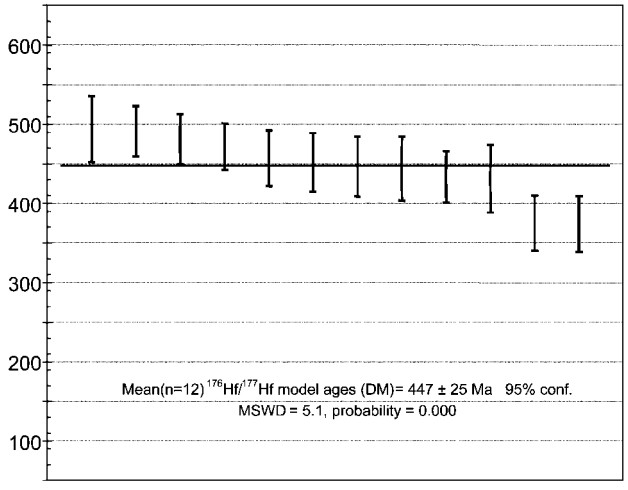

Figure 10. Weighted-average diagram for Hf model age data (n = 12) obtained from SC1 and RO/RB29, using LAM-MC-ICPMS analyses of single zircon grains. *MSWD* = mean squares of weighted deviates.

veins with subgreenschist facies assemblages and associated epidotization/cataclasis indicate that parts of the original island arc–back-arc assemblage were raised to and deformed at lower temperatures at higher crustal levels. The timing of this uplift event is not known but is most likely to be the Middle Permian Hunter-Bowen Orogeny that is responsible for the folding and faulting in the Paleozoic arc-forearc basin sequences (Veevers 2000).

Paleozoic History of the SNEFB. The Paleozoic history of the NEFB and particularly the associated Lachlan Fold Belt (fig. 14) has been discussed by a number of authors (Murray 1997 and references therein; Gray and Foster 2004). In the SNEFB, earlier petrographic and more recent geochemical, paleontological, and radiogenic isotope studies have revealed island arc–related activity during the Early Cambrian (U-Pb zircon, 530 Ma [Aitchison and Ireland 1995]; Sm-Nd, 536 ± 28 Ma [Sano et al. 2004]) and Middle or early Late Cambrian (Cawood 1976; Stewart 1995; Leitch and Cawood 1996). It continued in the Early Ordovician (U-Pb zircon, 479 Ma; Fanning et al. 2002), Early Silurian (U-Pb zircon, 436 Ma; Kimbrough et al. 1993), Late Silurian to Middle Devonian (Cawood and Flood 1989; Aitchison and Flood 1995; Offler and Gamble 2002), and Late Devonian (Greentree 1998). Recent paleontological studies of marine sequences with arc basin affinities adjacent to the PMFS confirm the earlier studies and show that the sequences vary in age from Middle Cambrian to Late Ordovician (Furey-Greig et al. 2000; Furey-Greig 2003*a*, 2003*b*).

This study provides evidence for arc magmatism at the end of the Late Ordovician and links all the early Paleozoic arc–related events recognized previously. Thus, subduction-related island arc volcanism/plutonism occurred off the eastern margin of Gondwana continuously from the Cambrian to the end of the Devonian, revealing a more complete history of the SNEFB at this time than shown in recent paleogeographic reconstructions (e.g., Li and Powell 2001). There is general agreement that in the Early Carboniferous, the tectonic setting changed as a result of the accretion of intraoceanic island arcs to Gondwana (Aitchison et al. 1992), leading to the development of a continental calc-alkaline arc that remained active until the end of the Carboniferous (Roberts et al.1995; Scheibner and Basden 1998). At that time, slab rollback took place, leading to the creation of a new arc in the accretion-subduction complex of the SNEFB, approximately 250 km to the east of the former arc (Jenkins et al. 2002 and references therein).

Tectonic Blocks: Derivation and Timing of Transportation. Plate-tectonic models of the NEFB suggested by various authors involve the subduction and accretion of the Paleo-Pacific plate to the Australian continent during the Paleozoic (Leitch 1974; Scheibner and Basden 1998 and references therein).

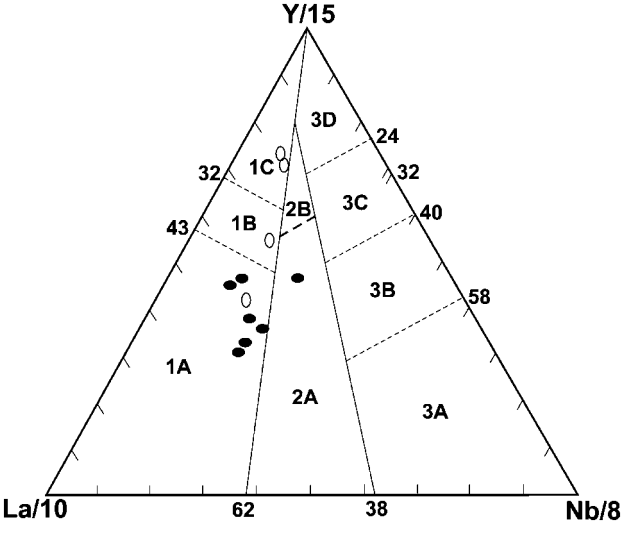

Figure 11. La/10-Y/15-Nb/8 discrimination diagram of Cabanis and Lecolle (1989). Samples are the same as those in figure 5. 1*A*, Calc-alkaline basalts; 1*B*, overlap between 1*A* and 1*C*; 1*C*, volcanic arc tholeiite; 2*A*, continental basalts; 2*B*, back-arc basin basalts; 3*A*, alkali basalts from intercontinental rift; 3*B*–3*C*, enriched mid-ocean ridge basalt (MORB); 3*D*, normal MORB. Samples of cumulate origin are not included.

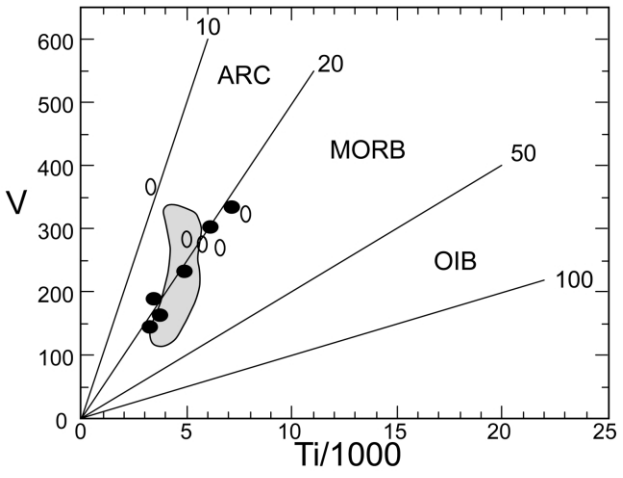

Figure 12. V-Ti/1000 discrimination plot of Shervais (1982). Shaded area indicates calc-alkaline rocks. Samples of cumulate origin are not included. Symbols used are the same as those in figure 5.

In the SNEFB, the PMFS forms a fundamental structural element ~350 km in length separating the Silurian to lower Carboniferous accretion-subduction complex sequences of the Tablelands Complex on the east from the upper Silurian to Carboniferous arc and forearc sequences of the Tamworth Belt on the west (fig. 1). Thrust and subsequent left lateral displacement on the PMFS has been postulated (Corbett 1976; Offler and Williams 1987; Cao and Durney 1993); the latter appears to have taken place before the emplacement of the Moonbi Adamellite (247–249 Ma; Shaw 1994), a stitching pluton cutting the Peel Fault (Collins 1991 and references therein). The PMFS has been interpreted by some as the suture along which subduction occurred (Blake and Murchey 1988) or as an ancestral fault system that formed during the initial subduction process (Collins 1991). Recent seismic studies of the SNEFB, however, have revealed the presence of a moderately west-dipping reflection to the east of the Peel Fault that appears to intersect this structure at shallow crustal levels (Korsch et al. 1997). According to Korsch et al. (1997), the serpentinites emplaced along the Peel Fault were derived at depth from this west-dipping structure. If this interpretation is correct, the incorporation and transport of the tectonic blocks in the serpentinite mélange took place on this structure and were subsequently transported to higher crustal levels along the PMFS. The presence of tectonic blocks of Cambrian to Late Ordovician age incorporated in a serpentinite mélange derived from ophiolites with a supra-subduction zone affinity (Aitchison and Ireland 1995) supports this interpretation.

Age of the Crust and Mantle beneath the Southen New England Fold Belt. The New England and Lachlan Fold Belts developed as part of the Tasman Fold Belt System (Scheibner and Veevers 2000), which was initiated during the breakup of Rodinia (Direen and Crawford 2003). The time of breakup is considered to be between 830 and 730 Ma, with a second rifting event between 600 and 585 Ma (Direen and Crawford 2003).

To date, the Attunga eclogite (Shaw and Flood 1974), with a U-Pb zircon igneous crystallization age of ca. 650 Ma (Watanabe et al. 1998), is the oldest rock found in the SNEFB. Further, a metamorphic age of ca. 536 ± 18 Ma (Fanning et al. 2002) from the same zircons in the eclogite indicates that subduction was already well established by the Early Cambrian. Sm-Nd studies of a diorite block in the PMFS confirm this age (Sm-Nd isochron, 536 ± 38 Ma; Sano et al. 2004). By contrast, the oldest rocks found in the northern NEFB have ages of 562 ± 22 Ma (Sm-Nd isochron; Marlborough ophiolite; Bruce et al. 2000). These data suggest that the NEFB developed on oceanic crust at least late Neoproterozoic in age. Rb/Sr and Nd/Sm isotope studies of S- and I-type granitoids and sediments from the New England Batholith in the SNEFB (Hensel et al. 1985) indicate a crustal source possibly as old as Late Proterozoic. More recently, Hf isotopic data obtained by Flood and Shaw (2001)

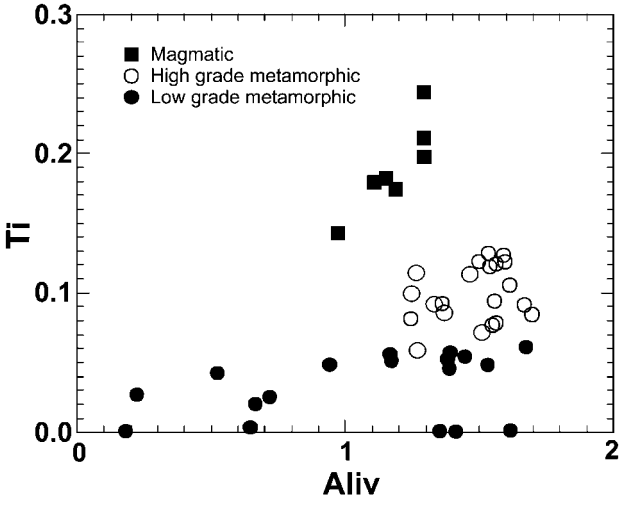

Figure 13. Ti-Al^{iv} plot of magmatic and metamorphic amphiboles. Note that Ti and Al^{iv} decrease from magmatic to low-grade metamorphic amphiboles. Symbols are as in figure 4.

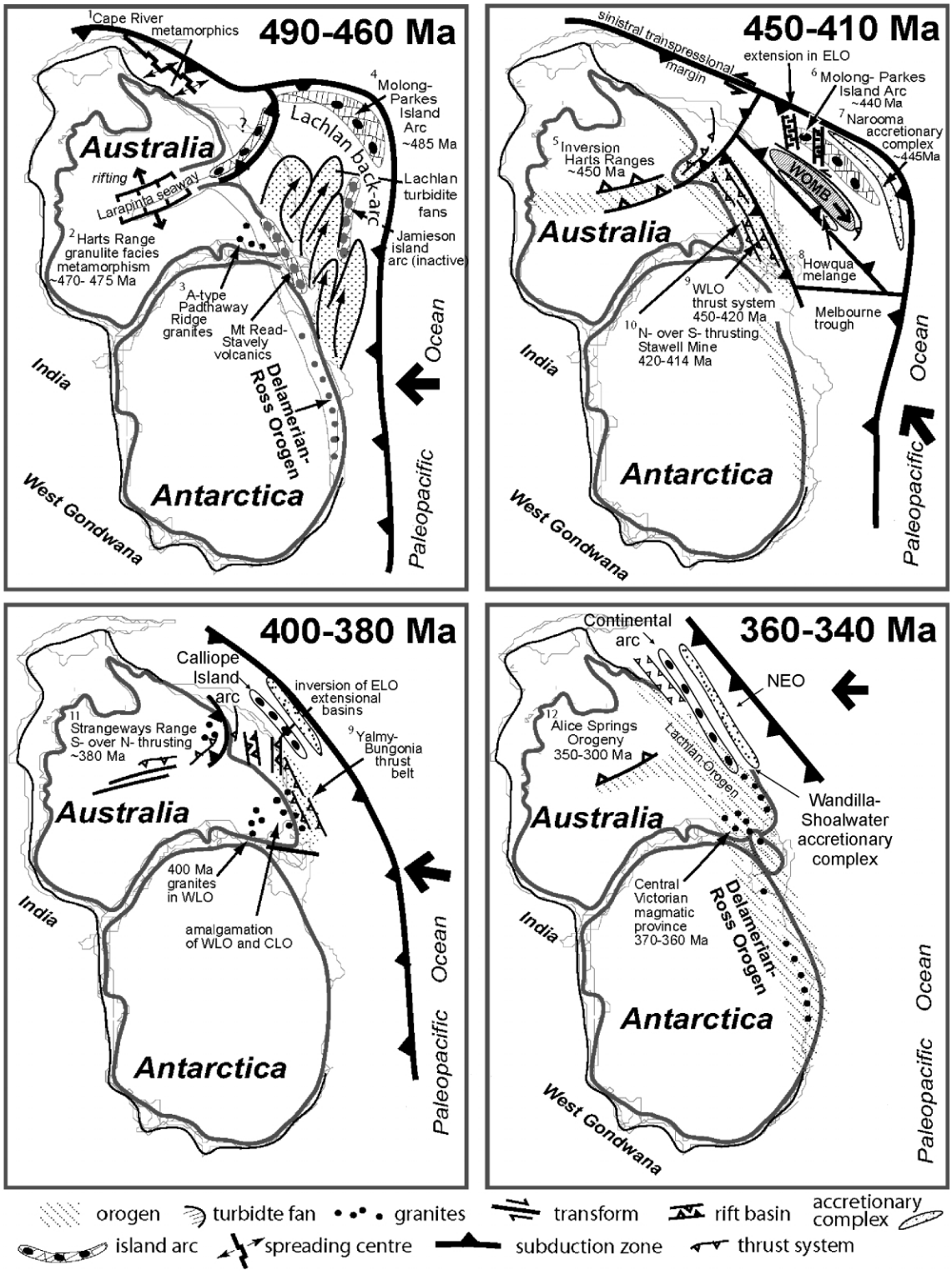

Figure 14. Proposed tectonic evolution for the Australia-Antarctica part of the Gondwana margin during the early to middle Paleozoic. Modified from Gray and Foster (2004). *WLO* = western Lachlan Orogen; *CLO* = central Lachlan Orogen; *ELO* = eastern Lachlan Orogen; *NEO* = New England Orogen (synonymous with New England Fold Belt); *WOMB* = Wagga-Omeo Metamorphic Belt. The Tablelands Complex forms the southern part of the Wandilla-Shoalwater accretionary complex. The alterations to the 400–380-Ma and 360–340-Ma time periods follow Scheibner and Veevers (2000) and Bryan et al. (2004).

and Shaw and Flood (2002) reveal T_{DM} ages varying from 870 to 250 Ma, from single zircons extracted from the I-type Moonbi Supersuite pluton. The older ages are consistent with magma being derived from source rocks that may be as old as Late Proterozoic. Similar ages have been obtained from spinel peridotite xenoliths in Tertiary basalts from the Tablelands Complex and the Tamworth Belt of the SNEFB (Powell et al. 2004). Re-Os isotope analyses of sulfides in these rocks revealed Re depletion model ages that are Proterozoic or older. The consistency of Proterozoic model ages obtained from Nd, Hf, and Re data, and the U-Pb and Sm-Nd isotopic data suggest that much of the crust and mantle of New England was associated with the breakup of Rodinia and initiation of the Pacific plate. The availability of this more recent data than existed previously allows for a better understanding of the nature of the crust in the SNEFB.

Conclusions

Major-element, trace-element, and REE analyses of deformed hornblende gabbros from a large tectonic block in a serpentinite mélange in the Glenrock Station area, New South Wales, have revealed that the rocks have a calc-alkaline magmatic affinity and a composition transitional between intraoceanic and continental arc rocks and that dikes associated with them have both calc-alkaline and tholeiitic back-arc basin basaltic arc composition. Cumulate layering and the presence of relict magmatic plagioclase, Ti-rich, Cl-bearing hornblende, and rare clinopyroxene with low Al^{vi} contents suggests that the original magma was strongly hydrous, contained minor quantities of Cl, and crystallized as a hornblende gabbro in a shallow crustal chamber.

Subsequent deformation occurred at peak metamorphic conditions of ~590°C and pressures of 550 MPa, producing a tectonic layering (S_1) defined by hornblende wrapping around partly recrystallized, magmatic plagioclase in the hornblende gabbro and, under high strain, an amphibolite with leucosomes. Continuing deformation at higher crustal levels led to the replacement of both magmatic and high-grade metamorphic minerals by lower amphibolite and, finally, prehnite-pumpellyite facies assemblages.

Zircon U-Pb analyses yielded a combined Late Ordovician age of 444.7 ± 2.4 Ma (2σ) in accordance with Lu-Hf T_{DM} model ages from the same samples (447 ± 25 Ma [2σ]). The similarity of zircon crystallization ages and T_{DM} model ages suggests little if any crustal residence between the time of partial melting of depleted mantle to produce the gabbro magma and the time of zircon crystallization. This study provides evidence for Late Ordovician arc magmatism and links all the Early Paleozoic arc–related events recognized previously. It further shows the value of studying tectonic blocks to decipher the geological history of fold mountain belts.

ACKNOWLEDGMENTS

We thank R. Flood for his constructive comments on the original manuscript. Our thanks also to Y. Y. Sun and Z. Jiang for preparation of thin sections, fused disks, pressed mounts, and drafting. D. Phelan provided assistance with EDS analyses, J. Zobec with XRF analyses, and R. Bale with collection of samples in the field and with drafting. We also thank D. Jenkins and an anonymous reviewer, D. Gray for providing a figure from one of his papers, and B. Schulz for providing a spreadsheet of the thermobarometer.

REFERENCES CITED

Aitchison, J. C.; Blake, M. C., Jr.; Flood, P. G.; and Jayko, A. S. 1994. Paleozoic ophiolitic assemblages within the southern New England Orogen of eastern Australia: implications for growth of the Gondwana margin. Tectonics 13:1135–1149.

Aitchison, J. C., and Flood, P. G. 1995. Gamilaroi Terrane: a Devonian rifted intra-oceanic island-arc assemblage, NSW, Australia. *In* Smellie, J. L., ed. Volcanism associated with extension at consuming plate margins. Geol. Soc. Spec. Publ. 81:155–168.

Aitchison, J. C.; Flood, P. G.; and Spiller, F. C. P. 1992. Tectonic setting and paleoenvironment of terranes in the southern New England Orogen, eastern Australia as constrained by radiolarian biostratigraphy. Palaeogeogr. Palaeoclimatol. Palaeoecol. 94:31–54.

Aitchison, J. C., and Ireland, T. R. 1995. Age profile of ophiolitic rocks across the late Palaeozoic New England Orogen, New South Wales: implications for tectonic models. Aust. J. Earth Sci. 42:11–23.

Aitchison, J. C.; Stratford, J. M. C.; and Buckman, S. 1997. Geology of the Upper Barnard region: evidence of Early Permian oblique-slip faulting along the Peel-Manning Fault System. *In* Ashley, P. M., and Flood, P. G., eds. Tectonics and metallogenesis of the New England Orogen. Geol. Soc. Aust. Spec. Publ. 19:188–196.

Allen, A. D., and Leitch, E. C. 1992. The nature and origin of eclogite blocks in serpentinite from the Tamworth Belt, New England Fold Belt, eastern Australia. Aust. J. Earth Sci. 39:29–35.

Belousova, E. A.; Griffin, W. L.; O'Reilly, S. Y.; and Fisher,

N. I. 2002. Igneous zircon: trace element composition as an indicator of source rock type. Contrib. Mineral. Petrol. 143:602–622.

Belousova, E. A.; Griffin, W. L.; and Pearson, N. J. 1998. Trace element composition and cathodoluminescence properties of southern African kimberlitic zircons. Mineral. Mag. 62:355–366.

Benson, W. N. 1913. The geology and petrology of the Great Serpentine Belt of New South Wales. Proc. Linn. Soc. N.S.W. 38:662–724.

Blake, M. C., Jr., and Murchey, B. L. 1988. A Californian model for the New England Fold Belt. Geol. Surv. N.S.W. Q. Notes 72:1–9.

Bruce, M. C.; Niu, Y.; Habort, T. A.; and Holcombe, R. J. 2000. Petrological, geochemical and geochronological evidence for a Neoproterozoic ocean basin recorded in the Marlborough terrane of the northern New England Fold Belt. Aust. J. Earth Sci. 47:1053–1064.

Bryan, S. E.; Allen, C. M.; Holcombe, R. J.; and Fielding, C. R. 2004. U-Pb zircon geochronology of Late Devonian to Early Carboniferous extension: related silicic volcanism in the northern New England Fold Belt. Aust. J. Earth Sci. 51:645–664.

Cabanis, B., and Lecolle, M. 1989. Le diagramme La/10-Y/15-Nb/8: un outil pour la discrimination des series volcaniques et la mise en evidence des processes de mélange et/ou de contamination crustale. C. R. Acad. Sci. II 309:2023–2029.

Cao, X. N., and Durney, D. W. 1993. Folding and cleavage in the eastern Tamworth Belt, Manilla. *In* Flood, P., and Aitchison, J. C., eds. New England Orogen, Eastern Australia Conference (Armidale, Australia, 1993), Proc., p. 255–256.

Cawood, P. A. 1976. Cambro-Ordovician strata, northern New South Wales. Search 7:317–318.

Cawood, P. A., and Flood, R. H. 1989. Geochemical character and tectonic significance of Early Devonian keratophyres in the New England Fold Belt, eastern Australia. Aust. J. Earth Sci. 36:297–311.

Collins, W. J. 1991. A reassessment of the Hunter-Bowen Orogeny: tectonic implications for the southern New England Fold Belt. Aust. J. Earth Sci. 38:409–423.

Colombi, A. 1989. Métamorphisme et géochimie des roches mafiques des Alpes oueste-centrales (géoprofile Viège-Domodossola-Locarno). Mem. Geol. 4:1–216.

Corbett, G. J. 1976. A new fold structure in the Woolomin Beds suggesting a sinistral movement on the Peel Fault. J. Geol. Soc. Aust. 23:401–406.

Corfu, F.; Hanchar, J. M.; Hoskin, P. W. O.; and Kinny, P. 2003. Atlas of zircon textures. *In* Hanchar, J. M., and Hoskin, P. W. O., eds. Zircon. Rev. Mineral. Geochem. 53:469–500.

Cowan, D. S. 1978. Origin of blueschist-bearing chaotic rocks in the Franciscan Complex, San Simeon, California. Geol. Soc. Am. Bull. 89:1415–1423.

Cross, K. C. 1983. The Pigna Barney Ophiolitic Complex and associated basaltic rocks, northeastern New South Wales. PhD thesis, University of New England, Armidale, Australia.

DeBari, S. M., and Coleman, R. G. 1989. Examination of the deep levels of an island arc: evidence from the Tonsina ultramafic-mafic assemblage, Tonsina, Alaska. J. Geophys. Res. 94:4373–4391.

De Jesus, J. V.; Yumul, G. P., Jr.; and Faustino, D. V. 2000. The Cansiwang Melange of southeast Bohol (central Philippines): origin and tectonic implications. Island Arc 9:565–574.

Direen, N. G., and Crawford, A. J. 2003. The Tasman Line: where is it, what is it, and is it Australia's Rodinian breakup boundary? Aust. J. Earth Sci. 50:491–502.

Ernst, G. W. G., and Liu, J. 1998. Experimental phase-equilibrium study of Al- and Ti-contents of calcic amphibole in MORB: a semiquantitative thermobarometer. Am. Mineral. 83:952–969.

Fanning, C. M.; Leitch, C. E.; and Watanabe, T. 2002. An updated assessment of the SHRIMP U-Pb Zircon dating of the Attunga eclogite in New South Wales, Australia: relevance to the Pacific Margin of Gondwana. International Symposium on the Amalgamation of Precambrian Blocks and the Role of the Palaeozoic Orogens in Asia (Sapporo, 2002).

Flood, R. H., and Shaw, S. E. 2001. The S-type granite source-rock debate: possible additional felsic component formed by fractionation of mantle derived mafic heat-source magmas. *In* Chappell, B. W., and Fleming, P. D., eds. 2001 S-type granites and related rocks. Aust. Geol. Surv. Org. Rec. 2001/2002, p. 41–42.

Fukui, S.; Watanabe,T.; Itaya, T.; and Leitch, E. C. 1995. Middle Ordovician high *PT* metamorphic rocks in eastern Australia: evidence from K-Ar ages. Tectonics 14:1014–1020.

Furey-Greig, T. G. 2003*a*. *Hirstodontus daleki*: a new Late Ordovician conodont species from the Wisemans Arm Formation, Eastern Australia. Cour. Forschungsinst. Seckenb. 245:421–425.

———. 2003*b*. Middle Ordovician conodonts from the Haedon Formation, north-eastern New South Wales. Cour. Forschungsinst. Seckenb. 245:315–325.

Furey-Greig, T. G.; Leitch, E. C.; and Cawood, P. A. 2000. Early Palaeozoic arc basin sequence in the Tamworth Belt: constraints for east Gondwana tectonics. Australian Geological Convention, 15th (Sydney, 2000). Geol. Soc. Aust. Abstr. 59:163.

Gamble, J. A.; Smith, I. E. M.; McCulloch, M. T.; and Kokkelaar, B. P. 1993. The geochemistry and petrogenesis of basalts from the Taupo Volcanic Zone and Kermadec Island Arc, SW Pacific. J. Volcanol. Geotherm. Res. 54:265–290.

Gerya, T. V.; Perchuk, L. L.; Triboulet, C.; Audren, C.; and Sez'ko, A. I. 1997. Petrology of the Tumanshet Zonal Metamorphic Complex, eastern Saya. Petrologiya 5:563–595.

Gray, D. R., and Foster, D. A. 2004. Tectonic evolution of the Lachlan Orogen, south-east Australia: a historical review, data synthesis and modern perspectives. Aust. J. Earth Sci. 51:773–817.

Greentree, M. R. 1998. The Keepit Volcano: a source for the Devonian Mostyn Vale and Baldwin Formations? BS thesis, Macquarie University, Sydney.

Griffin, W. L.; Pearson, N. L.; Belousova, E.; Jackson,

S. E.; van Achterbergh, E.; O'Reilly, S. Y.; and Shee, S. R. 2000. The Hf isotope composition of cratonic mantle: LAM-MC-ICPMS analysis of zircon megacrysts in kimberlites. Geochim. Cosmochim. Acta 64:13–147.

Hanchar, J. M., and Watson, E. B. 2003. Zircon saturation thermometry. *In* Hanchar, J. M., and Hoskin, P. W. O., eds. Zircon. Rev. Mineral. Geochem. 53:89–112.

Helz, R. T. 1973. Phase relations of basalts in their melting range at P_{H_2O} = 5 kb as a function of oxygen fugacity. I. Mafic phases. J. Petrol. 14:249–302.

Hensel, H.-D.; McCulloch, M. T.; and Chappell, B. W. 1985. The New England Batholith: constraints on its derivation from Nd and Sr isotopic studies of granitoids and country rocks. Geochim. Cosmochim. Acta 49:369–384.

Holland, T., and Blundy, J. 1994. Non-ideal interactions in calcic amphiboles and their bearing on amphibole-plagioclase thermometry. Contrib. Mineral. Petrol. 116:433–447.

Jackson, S. E.; Horn, I.; Longerich, H. P.; and Dunning, G. R. 1996. The application of laser ablation microprobe (LAM)-ICP-MS to in situ U-Pb zircon geochronology. V. M. Goldschmidt Conference, 6th. J. Conf. Abstr. 1:283.

Jenkins, R. B.; Landenberger, B.; and Collins, W. J. 2002. Late Palaeozoic retreating and advancing subduction boundary in the New England Fold Belt, New South Wales. Aust. J. Earth Sci. 49:467–489.

Johannes, W., and Holtz, F. 1996. The tonalite system Qz-Ab-An. *In* Johannes, W., and Holtz, F., eds. Petrogenesis and experimental petrology of granitic rocks. Berlin, Springer, p. 202–228.

Kent, A. J. R.; Peate, D. W.; Newman, S.; Stolper, E. M.; and Pearce, J. A. 2002. Chlorine in submarine glasses from the Lau Basin: seawater contamination and constraints on the composition of slab-derived fluids. Earth Planet. Sci. Lett. 202:361–377.

Kimbrough, D. L.; Cross, K. C.; and Korsch, R. J. 1993. U-Pb isotope ages for zircons from the Pola Fogal and Nundle granite suites, southern New England Orogen. *In* Flood, P., and Aitchison, J. C., eds. New England Orogen, Eastern Australia Conference (Armidale, Australia, 1993), Proc., p. 403–412.

Korsch, R. J.; Johnstone, D. W.; and Wake-Dyster, K. D. 1997. Crustal architecture of the New England orogen based on deep seismic reflection profiling. *In* Ashley, P. M., and Flood, P. G., eds. Tectonics and metallogenesis of the New England Orogen: Alan H. Voisey memorial volume. Geol. Soc. Aust. Spec. Publ. 19:29–51.

Laird, J., and Albee, A. L. 1981. Pressure, temperature and time indicators in mafic schist: their application to reconstructing the polymetamorphic history of Vermont. Am. J. Sci. 281:121–175.

Leake, B. E.; Woolley, A. R.; Arps, C. E. S.; Birch, W. D.; Gilbert, M. C.; Grice, J. D.; Hawthorne, F. C.; et al. 1997. Nomenclature of amphiboles: report on the Subcommittee on Amphiboles of the International Mineralogical Association, Commission on New Minerals and Mineral Names. Am. Mineral. 82:1019–1937.

Leitch, E. C. 1974. The geological development of the southern part of the New England Fold Belt. J. Geol. Soc. Aust. 21:133–156.

Leitch, E. C., and Cawood, P. A. 1996. Early Palaeozoic convergent margin elements in the New England Fold Belt and the inception of the Ring of Fire. Australian Geological Convention, 13th (Canberra, 1996), Geol. Soc. Aust. Abstr. 41:246.

Li, Z. X., and Powell, C. M. 2001. An outline of the palaeogeographic evolution of the Australasian region since the beginning of the Neoproterozoic. Earth Sci. Rev. 53:237–277.

Maekawa, H. 1989. Two modes of mixing of Biei ophiolite melange, Kamuikotan blueschist belt, Japan. J. Geol. 97:93–108.

Maruyama, S.; Liou, J. G.; and Terabayashi, M. 1996. Blueschists and eclogites of the world and their exhumation. Int. Geol. Rev. 38:485–594.

Murray, C. G. 1997. From geosyncline to fold belt: a personal perspective on the development of ideas regarding the tectonic evolution of the New England Orogen. *In* Ashley, P. M., and Flood, P. G., eds. Tectonics and metallogenesis of the New England Orogen: Alan H. Voisey memorial volume. Geol. Soc. Aust. Spec. Publ. 19:1–28.

Nozaka, T. 1999. Blueschist blocks at Mochimaru in the Tari-Misaka ultramafic complex: their petrologic characteristics and significance. Island Arc 8:154–167.

Offler, R. 1982. The origin of exotic blocks in serpentinites, Peel Fault System, Glenrock Station, NSW. *In* Flood, P. G., and Runnegar, B., eds. New England Geology. Armidale, Australia, University of New England, p. 43–51.

———. 1999. Origin of blueschist "knockers," Glenrock Station, NSW. *In* Flood, P. G., ed. New England Orogen regional geology, tectonics and metallogenesis. Armidale, Australia, University of New England, p. 35–44.

Offler, R., and Gamble, J. 2002. Evolution of an intra-oceanic island arc during the Late Silurian to Late Devonian, New England Fold Belt. Aust. J. Earth Sci. 49:349–366.

Offler, R., and Williams, A. 1987. Evidence for sinistral movement on the Peel Fault System in serpentinites, Glenrock Station, NSW. *In* Leitch, E. C., and Scheibner, E., eds. Terrane accretion and orogenic belts. Am. Geophys. Union Geodyn. Ser. 19:141–151.

Pearce, J. A. 1983. Role of sub-continental lithosphere in magma genesis at active continental margins. *In* Hawkesworth, C. J., and Norry, M. J., eds. Continental basalts and mantle xenoliths. Nantwich, UK, Shiva, p. 230–249.

———. 1996. A user's guide to basalt discrimination diagrams. *In* Wyman, D. A., ed. Trace element geochemistry of volcanic rocks: applications for massive sulphide exploration. Geol. Assoc. Can. Short Course Notes 12:79–113.

Powell, W.; O'Reilly, S.; and Alard, A. 2004. Defining age constraints for mantle events from Re-Os isotopes and tracking metasomatic processes in lithospheric mantle domains beneath New England. *In* McPhie, J., and

McGoldrick, P., eds. Dynamic earth: past, present and future. Geol. Soc. Aust. Abstr. 73:285.

Powell, W. G; Carmichael, D. M.; and Hodgson, C. J. 1995. Conditions and timing of metamorphism in the southern Abitibi greenstone belt, Quebec. Can. J. Earth Sci. 32:787–805.

Roberts, J.; Claoue-Long, J.; Jones, P. J.; and Foster, C. B. 1995. SHRIMP zircon age control of Gondwana sequences in late Carboniferous and Early Permian Australia. *In* Dunnay, R. E., and Hailwood, E. A., eds. Non-biostratigraphical methods of dating and correlation. Geol. Soc. Spec. Publ. 89:145–174.

Robinson, P.; Spear, F. S.; Schumacher, J. C.; Laird, J.; Klein, C.; Evans, B. W.; and Doolan, B. L. 1982. Phase relations of metamorphic amphiboles: natural occurrence and theory. *In* Veblen, D. R., and Ribbe, P. H., eds. Reviews in mineralogy. Vol. 9B. Chantilly, VA, Mineralogical Society of America, p. 1–227.

Sano, S.; Offler, R.; Hyodo, H.; and Watanabe, T. 2004. Geochemistry and chronology of tectonic blocks in serpentinite mélange of the southern New England Fold Belt, NSW, Australia. Gondwana Res. 7:817–831.

Scheibner, E., and Basden, H. 1998. Geology of New South Wales: synthesis. Vol. 2. Geological evolution. Sydney, Geological Survey of New South Wales, 666 p.

Scheibner, E., and Veevers, J. J. 2000. Tasman Fold Belt System. *In* Veevers, J. J., ed. Billion-year earth history of Australia and neighbours in Gondwanaland. Sydney, Centre for Geochemical Evolution and Metallogeny of Continents, p. 154–234.

Shaw, S. E. 1994. Late Permian-Triassic radiometric dates of granitoids and associated volcanics from the southern New England Fold Belt. *In* Veevers, J. J., and Powell, C. A., eds. Permian-Triassic Pangean basins and foldbelts along the Panthalassan margin of Gondwanaland. Geol. Soc. Am. Mem. 184:147–171.

Shaw, S. E., and Flood, R. H. 1974. Eclogite from serpentinite, near Attunga, New South Wales. J. Geol. Soc. Aust. 21:377–385.

———. 2002. A reconnaissance $^{176}Hf/^{177}Hf$ study of the New England Batholith using LAM-MC-ICPMS microanalysis of zircons. *In* Preiss, V. P., ed. Geoscience 2002: expanding horizons. Australian Geological Convention, 16th (Adelaide, 2002), Abstr. 67, p. 190.

Shervais, J. W. 1982. Ti-V plots and the petrogenesis of modern and ophiolitic lavas. Earth Planet. Sci. Lett. 59:101–118.

Spaggiari, C. V.; Gray, D. R.; and Foster, D. 2002. Occurrence and significance of blueschists in the southern Lachlan Orogen. Aust. J. Earth Sci. 49:255–269.

Stewart, I. 1995. Cambrian age for the Pipeclay Creek Formation, Tamworth Belt, northern New South Wales. Cour. Forschungsinst. Seckenb. 182:565–566.

Stratford, J. M. C., and Aitchison, J. C. 1997. Lithostratigraphy of the Gamilaroi Terrane, upper Barnard region, northeastern New South Wales. *In* Ashley, P. M., and Flood, P. G., eds. Tectonics and metallogenesis of the New England Orogen. Geol. Soc. Aust. Spec. Publ. 19: 178–187.

Sun, S.-S., and McDonough, W. F. 1989. Chemical and isotopic systematics of oceanic basalts: implications for mantle compositions and processes. *In* Saunders, A. D., and Norry, M. J., eds. Magmatism in the ocean basins. Geol. Soc. Spec. Publ. 42:315–345.

Tsujimori, T., and Itaya, T. 1999. Blueschist-facies metamorphism during Paleozoic orogeny in southwestern Japan: phengite K-Ar ages of blueschist-facies tectonic blocks in serpentinite mélange beneath early Paleozoic Oeyama ophiolite. Island Arc 8:190–205.

van Achterbergh, E.; Ryan, C. G.; Jackson, S. E.; and Griffin, W. L. 2001. Data reduction software for LA-ICP-MS. *In* Sylvester, P. J., ed. Laser ablation–ICP–mass spectrometry in the earth sciences: principles and applications. Mineral. Assoc. Can. Short Course Ser. 29: 239–242.

Veevers, J. J. 2000. Permian-Triassic Pangean basins and fold belts along the Panthalassan margin of eastern Australia. *In* Veevers, J. J., ed. Billion-year earth history of Australia and neighbours in Gondwanaland. Sydney, Centre for Geochemical Evolution and Metallogeny of Continents, p. 235–252.

Watanabe, T., and Iwasaki, M. 1988. Review and additional study of the high-pressure metamorphic rocks in the southern New England Fold Belt: preliminary report on the geology of the New England Fold Belt, No. 1., p. 95–109.

Watanabe, T.; Fanning, C. M.; and Leitch, E. 1998. Neoproterozoic Attunga eclogite in the New England Fold Belt. Australian Geological Society Convention, 14th (Townsville, Australia, 1998), Abstr. 49, p. 458.

Winchester, J. A., and Floyd, P. A. 1977. Geochemical discrimination of different magma series and their differentiation products using immobile elements. Chem. Geol. 20:325–343.

Wood, D. A. 1980. The application of a Th-Hf-Ta diagram to problems for tectonomagmatic classification and to establishing the nature of crustal contamination of basaltic lavas of the British Tertiary volcanic province. Earth Planet. Sci. Lett. 50:11–30.

Yang, K., and Seccombe, P. K. 1997. Geochemistry of the mafic and ultramafic complexes of the northern Great Serpentinite Belt, New South Wales: implications for first stage melting. *In* Ashley, P. M., and Flood, P. G., eds. Tectonics and metallogenesis of the New England Orogen. Geol. Soc. Aust. Spec. Publ. 19:197–211.

Zenk, M., and Schulz, B. 2004. Zoned Ca-amphiboles and related *P-T* evolution in metabasites from the classical Barrovian metamorphic zones in Scotland. Mineral. Mag. 68:769–786.